The DOI for this manuscript is doi: 10.1175/2009JCLI2757.1

Amazon deforestation and climate change in a coupled model simulation.

Paulo Nobre[1], Marta Malagutti, Domingos Urbano, Roberto de Almeida, and Emanuel Giarolla.

Centro de Ciências do Sistema Terrestre – CCST

Instituto Nacional de Pesquisas Espaciais – INPE

Submitted to: J. Climate

Revised form on

03 May 2009.

1 Corresponding author address: Paulo Nobre, INPE, Rodovia Presidente Dutra, Km 40, Cachoeira Paulista, SP 12630-000, BRAZIL, e-mail: pnobre@cptec.inpe.br

Abstract

The impacts of Amazon deforestation on climate change are investigated through the use of twin numerical experiments with an Atmospheric General Circulation Model (AGCM) with prescribed global sea surface temperature and the same AGCM coupled to an ocean GCM over the global-tropics (CGCM). An ensemble approach is adopted, with ten member ensemble-averages of a control simulation compared with perturbed simulations for three scenarios of Amazon deforestation. The latest 20 years of simulation from each experiment are analyzed. Local surface warming and rainfall reduction are simulated by both models over the Amazon basin, with the coupled model presenting rainfall reduction that is nearly 60% larger compared to its control run than those obtained by the AGCM. The results also indicated that both the fraction of the deforested area and the spatial continuity of vegetated area might be important for modulating global climate variability and change. Additionally, significant remote atmospheric responses to Amazon deforestation scenarios are detectable for the coupled simulations, which revealed global ocean and atmosphere circulation changes conducive to enhanced ocean-atmosphere variability over the Pacific Ocean. This, in turn, is interpreted as a manifestation of enhanced El Niño-Southern Oscillation (ENSO) activity over the Pacific and a positive feedback contributing to the extra rainfall reduction over the Amazon on the coupled simulations.

1 Introduction

Several studies have investigated the effects of Amazon deforestation on regional climate variability and change (e.g. Henderson-Sellers and Gornitz, 1984; Nobre et al., 1991; Zeng et al., 1996; Werth and Avissar, 2002; Voldoire and Royer, 2005; Schneider et al., 2006). Although the conclusions of such studies are dependent on a number of parameterized processes (e.g., convection schemes on Atmospheric General Circulation Models - AGCMs), there is a general agreement that Amazon deforestation leads to local reduction of rainfall and increase of surface temperature. Some studies also looked into the remote atmospheric response to Amazon (e.g. Werth and Avissar, 2002) or the global tropics (Findell et al., 2006) rainforest substitution for grass. The teleconnection responses to the extratropics, however, appear more variable and subtle than the local responses to deforestation. Of particular interest are the questions regarding the importance of ocean-atmosphere feedbacks to tropical forest clearing. Voldoire and Royer (2005) found no significant differences in local precipitation changes in Amazon deforestation experiments using either prescribed global Sea Surface Temperature (SST) or an interacting coupled ocean-atmosphere model. Schneider et al. (2006) utilized an anomaly coupled ocean-atmosphere general circulation model (CGCM), as well as coupled models of intermediary complexity, to study this aspect and concluded that ocean-atmosphere interactions are of secondary importance in modulating the local response of rainfall reduction due to deforestation. They argue that the local rainfall reduction and surface continental temperature increase over the Amazon region act in opposite directions to destabilize the atmosphere-ocean interface over the tropical Pacific – with surface warming leading to enhanced ENSO (El Niño-Southern Oscillation) conditions and precipitation reduction leading to damped ENSO conditions – with the surface temperature influence dominating.

In this study, an AGCM forced with climatological global SST and a CGCM coupled over the global tropics are used to investigate the sensitivity of ocean-atmosphere coupled simulations to extreme scenarios of Amazon deforestation, i.e., substitution of Amazon rainforest for savanna-type vegetation. Three arbitrary deforestation patterns and 10 member ensemble averages of both the CGCM and the AGCM forced with prescribed global SST are used to identify the ocean-atmosphere responses to scenarios of deforestation over the Amazon. Our results concur only partially with previous results, in the sense that deforestation leads to reduced rainfall and increased surface temperature over the Amazon region. In contrast, the numerical model results presented in this article suggest that the rainfall reduction over the Amazon is enhanced when the cooperation of ocean-atmosphere interactions are considered.

Section 2 describes the GCMs used and experiment design; Section 3 presents a discussion of the results

of both AGCM and CGCM integrations; conclusions and suggestions for further studies are presented in section 4.

2 Models and experiments description

The atmospheric component of the CGCM is the Centro de Previsão de Tempo e Estudos Climáticos' (CPTEC) spectral global model (Cavalcanti et al., 2002) with triangular truncation at wave number 62, and 28 unevenly spaced sigma levels in the vertical (T062L28). The surface scheme used is the Simplified Simple Biosphere Model - SSIB (Xue et al., 1991). Turbulence within the planetary boundary layer is parameterized through the closure scheme of Mellor-Yamada (1982). Short wave radiation is represented by the scheme of Lacis and Hansen (1974) modified by Ramaswamy and Freidenreich (1992) and is computed hourly. Long wave radiation is based on Harshvardhan et al. (1987) and is computed at 3 hour intervals. Convective precipitation is produced by the relaxed Arakawa-Schubert (RAS) scheme (Moorthi and Suarez, 1992).

The oceanic component of the CGCM is the Geophysical Fluid Dynamic's (GFDL) Modular Ocean Model version 3 (Pacanowski and Griffies, 1999). The model settings are basically the same as described by Giarolla et al. (2005). The domain covers the global tropics, between 40°N and 40°S. The horizontal grid has 0.25° latitudinal resolution between 10°S and 10°N over the global tropics, decreasing gradually to 2.75° degrees at 40°S and 40°N. The longitudinal resolution is 0.25° over the Atlantic, decreasing to 3.75° over both the Indian and Pacific Oceans. The model configuration has twenty levels in the vertical, spaced 15 m within the top 100 m. The lateral oceanic boundary conditions at 40°S and 40°N are zonal slip conditions with zero meridional flow at the boundaries. The vertical mixing scheme chosen is based on Pacanowski and Philander (1981). Surface heat fluxes for the OGCM forced runs are parameterized according to Rosati and Miyakoda (1988) bulk formulas. The model uses the rigid lid approximation on the ocean surface to filter out high frequency surface gravity waves.

The CGCM spin-up process consisted of initially integrating a single realization of the OGCM with prescribed momentum fluxes and parameterized surface heat fluxes for a total of 47 years in two segments; one, starting from Levitus (1982) temperature-salinity (T-S) initial conditions (IC) and forced by the European Centre for Medium Range Forecasting (ECMWF) surface wind stress analysis (Trenberth et al., 1989) and solar radiation (Oberhuber, 1988) monthly climatologies linearly interpolated to the day of integration for 30 years; and the other consisting of integrating the single realization of the OGCM forced by interannually varying monthly surface wind stress fields from the National Center for Atmospheric Research (NCAR)/National Centers for Environmental Prediction (NCEP) reanalysis for

additional 17 years. From this point, the CGCM is spun-up for a period of 12 years in ensemble mode for each deforestation scenario and control. The ocean ICs for the coupled spin-up are all from the single OGCM run, while the AGCM ICs are daily NCEP reanalysis for December 16-25, 1987. The dates chosen are such as to coincide with the end of the OGCM forced spin-up period. The spin-up interval of the AGCM is two years from the same set of atmospheric IC fields used to initialize the CGCM spin-up runs and are also done for each deforestation and control scenarios.

The atmospheric and oceanic GCMs are coupled through the fields: SST, computed by the ocean model; and total heat flux (i.e., +solar – latent – sensible – longwave), zonal and meridional momentum fluxes, and precipitation minus evaporation (simulating a salt flux) computed by the atmospheric model. The coupling interval is daily and no flux correction is applied. Oceanic boundary conditions for the uncoupled runs and for the coupled runs poleward of 40° North and South are monthly varying climatological optimum interpolation OI-SST (Reynolds et al., 2002).

Empirical Orthogonal Function analysis (EOF) (Lorenz, 1956; Preisendorfer, 1988) are used to detect the leading patterns of variability of Sea Surface Temperature Anomalies (SSTA) and Surface Wind Stress Anomalies (SWSA). Anomalies of each variable were normalized by their respective standard deviation at each grid point, to grant the same importance to variables/areas with varying degrees of variability (e.g., Nobre and Shukla, 1996).

2.1 Experiment design

After the spin-up process described above, 10 members, 20 year long pairs of ACGM and CGCM runs were done for the four Amazon vegetation scenarios shown in Figure 1 and described below. Additionally, one member of the CGCM were integrated for additional 70 years to complete a single 90 years long run for each experiment. The control runs (hereafter referred to as CTRL) use the vegetation types of CPTEC's AGCM (Figure 1a) described by Xue et al. (1991, see their Table 2). The perturbed experiments use an idealized checkerboard deforestation pattern, with 50% deforested area in 1.85° x 1.85° squares (i.e., the native resolution of the AGCM; Figure 1b – hereafter referred to as DFOR1), 50% deforested area in 5.5° x 5.5° squares (Figure 1c – DFOR2), and one single square area with 100% savanna (Figure 1d – DFOR3). Here, it shall be stated that the deforestation patterns used in each scenario are not intended to reproduce deforestation patterns either observed at the present or projected for the future over the Amazon region. Rather, they are aimed at constructing a first order sensitivity experiment to gauge the relative importance of deforested areas when interactive ocean-atmosphere exchanges are considered.

Throughout the text, the term “departure” refers to the residual of a particular deforestation experiment minus its twin control run; while the term “anomaly” refers to the residual of a particular deforestation experiment minus its own long term monthly mean. Where applicable, the statistical significance of the departures are assessed using a two-tail t-test ($p < 0.05$) comparing the control run with the deforestation experiments. The effective number of degrees of freedom used in the t-test is calculated considering the auto-correlation of the variable anomalies from the seasonal cycle of the corresponding experiment (see a detailed explanation by Stephenson and Benestad, 2009).

3 Results

First we comment on the CGCM behavior for the extended single-member runs done for the CTRL and the DFOR3 scenarios. Two approaches are used; one, in which the CGCM has been integrated for continuous 90 years after spinup; and the other, in which the ten members, 20 years long each, were concatenated to form one single 200 year-equivalent run (hereafter referred to as 90-year and 200-year runs, respectively). These runs are aimed at testing whether the CGCM presented sustained oscillations and trends on a centennial time scale. Regarding trends, no significant long term trends were detected in the 90-year runs, with the largest deviations found in the precipitation fields, of the order of 0.2 mm per decade over the equatorial Atlantic and -0.2 mm/decade over the eastern equatorial Pacific region (figures not shown).

Regarding oscillations, the CGCM presented irregular oscillatory behavior for the whole period of integration with maximum variability over the central-eastern equatorial Pacific, as depicted by the first eigenvector of the joint EOF (JEOF) of SSTA-SWSA for the 200-year CTRL run shown in Figure 2a. The global tropics pattern shown in Figure 2 depicts positive values of SSTA associated with weaker equatorial and trade winds over the central-eastern Pacific, and negative values of SSTA over the extra-tropics and western Pacific. The eigen-analyses of global tropics SSTA (figures not shown), as well as the JEOF of SSTA and SWSA for both the 90-year and the 200-year runs presented very similar results, with the first JEOF of SSTA-SWSA eigenvector for the 200-year run of the CTRL experiment (Fig. 2a) accounting for 14.7% of the combined variables total variance and presented as correlation maps. The first JEOF of SSTA-SWSA for the DFOR3 (figure not shown), also for the 200-year run, displays a similar spatial pattern as that shown in Figure 2a and explains 15.1% variance fraction. Figure 2b shows the power spectra of the eigenvector shown in Figure 2a for the CTRL (continuous line) and for the DFOR3 (dashed line) experiments. The increased energy power spectra in the range of three-to-four years

for the total deforestation scenario relative to that of the CTRL run (Fig. 2b) is an indication not only that the CGCM is capable to generating an ENSO-like mode of variability over the Pacific, but also that this mode of variability might be amplified by atmospheric teleconnections due to Amazon deforestation.

Despite the apparent capability of the CGCM to generate global oscillations resembling ENSO signal in the anomaly fields, the CGCM long runs presented some chronic deficiencies, namely a warm SST bias up to 4° C over the eastern Pacific and Atlantic basins (figures not shown), which saturated during the first three years of model integration, and are a common defect of coupled ocean-atmosphere global models (e.g. Richter and Xie, 2008).

Figure 3 shows the ensemble mean climatological rainfall annual cycle over the central Amazon for AGCM/CGCM outputs and observations. Two aspects are noteworthy in Figure 3; one, is the closer agreement of the CGCM CTRL run precipitation annual cycle (continuous line in Fig. 3b) with observations (red line in Figures 3 a,b) when compared with the excess rainfall shown by the AGCM (Fig. 3a). We speculate that the CGCM eastern oceans SST warm bias might possibly contribute to partially offset the excess rainfall produced by the AGCM convective scheme over Amazonia, through enhanced walker-cell subsidence over the region. Two, that climatologically wise the local effect of Amazon deforestation is to reduce the total monthly climatological rainfall over the region (dashed lines in Figs. 3 a,b), with the largest deviations for the DFOR3 experiment of total deforestation, both for the AGCM and CGCM runs. Another point of interest in Figure 3 is the systematic difference between climatological precipitation for experiments DFOR1 and DFOR2 for the CGCM, with the earlier presenting larger rainfall reduction than the latter. This is a rough indication that the details of deforestation spatial structure (in this case represented by the size of deforested mesh) might play a role on the local rainfall, when ocean-atmosphere interactions are considered.

Next we analyze the ensemble results for the twenty years-long runs, noting that the ensemble averaging smooths out high frequency natural variability of the time series. Figure 4 shows the time series of the area averaged rainfall departures ensemble means over the Amazon (Fig. 4 a,c) and the Niño 3.4 area (Fig. 4 b,d) for the AGCM (Fig. 4 a,b) and the CGCM (Fig. 4 c,d). Reproducing previous works, the local responses to deforestation in both AGCM and CGCM results are the reduction of rainfall totals throughout the integration period. Such differences between CTRL and deforested runs are also evident in the comparisons of precipitation long-term means annual cycles shown in Figure 3. However, it is clearly seen in both Figures 3 and 4, that the CGCM deforestation runs show local rainfall reductions over the Amazon that are consistently larger than those for the respective AGCM runs, with departures as large as 3.3 mm/day for the DFOR3 experiment, corresponding to approximately 42% reduction compared to the

CGCM CTRL run, which contrasts with the AGCM's 26% reduction for the total deforestation scenario (see Table 1). It is also noteworthy in Figure 4 and Table 1 that the rainfall reduction over the Amazon bears some proportionality to the area of rainforest substitution for savanna, with the largest departures occurring with the DFOR3 experiments, both for the AGCM and the CGCM runs. However, it should be noted that a linear reduction of precipitation with deforested area is a feature of coarse GCM simulations, but not in high resolution regional simulations of deforestation (e.g. Ramos da Silva et al., 2008), in which small-scale gradients in deforestation are resolved.

The effect of the interacting ocean is also highlighted when comparing the same percentage of rainforest removal but with different vegetated/deforested mesh cell sizes, as it is the case for experiments DFOR1 and DFOR2. The AGCM rainfall reduction over the Amazon for the smaller mesh size of DFOR1 scenario is of the order of 1.5% larger than for the DFOR2, while the CGCM difference between the two scenarios is four times as large (see Table 1). Noting also that DFOR1 ocean circulation departures over the equatorial Pacific (figures not shown) are second only to the total deforestation case DFOR3, it is plausible to think that not only the total deforested area, but also the extent of continuous forest tracts are relevant to organize convection over the Amazon and its effects on the global climate system, when the coupling with the oceans is considered.

Also in Figure 4, note that both AGCM and CGCM rainfall reductions over the Amazon (panels a and c) are nearly invariant throughout the period of model integration, but not for the CGCM rainfall departures over the Niño 3.4 area (Fig. 4d). Such time invariance over the Amazon contrasts with the rainfall departures over the equatorial Pacific for the Niño 3.4 area (Fig. 4 b,d) in two fundamental aspects. One, the AGCM results present nearly indistinguishable rainfall totals for each deforestation scenario and the CTRL experiment (denoted by the ensemble mean departures collapse toward the zero line in Fig. 4b). Two, the CGCM results present increased rainfall ensemble departures with considerable interannual variations, even after ensemble averaging (Fig. 4d). Table 1 summarizes the long term mean departures and standard deviations over both the Amazon and Niño 3.4 areas shown in Figure 4. Except for the AGCM DFOR2 scenario at the NINO 3.4 region, all departures are significantly different from zero at the 95% level. The comparison of panels b and d in Figure 4 and the respective standard deviations shown in Table 1 thus suggests that the AGCM response over the eastern equatorial Pacific to deforestation over the Amazon resembles a time series with a white noise spectrum (reason why the ensemble mean departures and their standard deviations tend to zero), while showing a large signal and considerable coherent interannual variability for the CGCM case during the integration period.

Figure 5 shows the statistically significant (i.e., non-statistically significant departures at the 95% level

are masked out) of the 20 year average,10 member ensemble mean precipitation and near surface air temperature departures for the DFOR3 experiment for the AGCM (Fig. 5a,b), CGCM (Fig. 5c,d) and the difference CGCM minus AGCM (Fig. 5e,f). It is noteworthy that the AGCM departures, both precipitation and temperature, are concentrated over the continental land masses while the CGCM results show extensive areas of positive and negative departures over the tropical oceans. Therefore, the differences of the atmospheric responses to Amazon deforestation for the AGCM and CGCM (Fig. 5e,f) reveal that not only the local rainfall reduction and surface temperature increase over the Amazon is larger for the coupled model results, but also the ensemble mean precipitation and temperature increase over the eastern equatorial Pacific are inherently coupled ocean-atmosphere responses to the prescribed Amazon deforestation.

3.1 Upper ocean circulation changes

This section evaluates the impact of Amazon deforestation on the tropical upper ocean circulation using the DFOR3 and CTRL CGCM runs. We expect that replacing tropical rain forest by savanna will lead to changes in the atmospheric circulation, affecting the trade winds system over the tropical oceans, affecting the upper ocean circulation. Particularly in the tropics, the lower branches of the large scale atmospheric circulation cells, i.e., trades and consequently the Inter-Tropical Convergence Zone (ITCZ) play an important role in modulating the strength and position of the main surface and subsurface ocean currents, depth of thermocline, upwelling/downwelling, and therefore SST (Katz, 1987; Xie, 1994).

The CTRL run is used to describe the general ocean circulation (Fig. 6a, thick black line; Fig. 6b, black contours), while the departures of experiment DFOR3 minus CTRL (Fig. 6a, continuous blue line and dashed red line; Fig. 6b, shades) are used to evaluate the impact of Amazon deforestation on atmospheric and ocean circulation. For the sake of clarity, we compare the speed ($||V||=(u^2+v^2)^{1/2}$) instead of horizontal velocity components to avoid alternating directions of flow. Therefore, all positive departures mean the flow has larger kinetic energy in the DFOR3 experiment compared with the CTRL and the opposite for negative departures.

The DFOR3 experiment shows weaker trade winds in almost all latitudes from 20°S to 20°N (Fig. 6a, red dashed line). As a response of these weaker winds, the ocean surface flow is weaker at the equator, in the northern branch of the South Equatorial Current (nSEC) region (Fig. 6a, blue line). Poleward of both SEC and North Equatorial Current (NEC) the ocean velocities are negative but close to zero due to positive values in the western Pacific. Out of the equatorial region a smaller zonal region must be used for analysis. Figure 6b shows the vertical distribution of the currents presented in Figure 6a. Shades represent

the current speed departures statistically significant at 95% level. It is noteworthy the strong weakening of the nSEC (negative values between 3°S and 3°N) and the upward displacement of the Equatorial Undercurrent (EUC) core, depicted by the area of intensification above the thermocline and weakening below it.

An important ocean circulation change related to Amazon deforestation is the EUC shallowing for the deforested case, shown in Figure 6b. The shallowing of the EUC results in more (less) eastward advection in the upper (lower) thermocline, which damps (lifts) the eastern (western) isotherms by the zonal advection of temperature. Also, the weakening of the lower EUC is related to the shallow Subtropical-Tropical Cells (STCs) that feed the EUC and are modulated by non-local westerly winds acting over subtropical regions (See: Snowden and Molinari, 2003 for a review on STCs).

Figure 7 displays the oceanic vertical velocity component (w) at 50 m depth from CTRL run (black contours) and the DFOR3 minus CTRL departures (shaded) statistically significant at 95% level. There is less upwelling (negative values) along the equator and less downwelling (positive) in the North Hemisphere, suggesting a less intense Tropical Cell (TC). Results from a Lagrangian trajectories analysis (De Vries and Döös, 2001) done with the results of the present work also confirm that the TCs and STCs are weaker in the deforestation experiment.

The changes in the ocean circulation due to Amazon rain forest depletion lead to changes in the ocean temperature field over the whole Pacific basin, as shown in Figure 8. The isotherms of DFOR3 experiment (dashed contours) are deeper than the CTRL (black contours) east of 160°W and shallower west of it. As a consequence, the eastern Pacific is up to 1°C warmer than the CTRL while in the west it is cooler by the same amount (shaded contours in Fig. 8), shifting the system closer to warm ENSO conditions. A detailed investigation of the intra-seasonal, annual and inter annual variability is necessary to understand the impact of Amazon deforestation on the Atlantic and Indian oceans, and shall be the subject of further study.

4. Conclusions

This study has investigated the role of ocean-atmosphere interactions on the climate change issue related to Amazon deforestation scenarios. The CGCM centennial single member CTRL and deforested integrations showed robust ENSO-like oscillations with maximum joint variability of SST and surface wind stress anomalies over the equatorial Pacific Ocean. The use of ten member ensembles of twin pairs of sensitivity numerical experiments with both AGCM and CGCM to identical Amazon deforestation scenarios revealed a significant role of global ocean-atmosphere interactions on both local and remote

climate change due to Amazon deforestation.

The AGCM ensemble response to Amazon deforestation reproduces previous results over the Amazon, i.e., local reduction of rainfall and surface temperature increase, but no significant remote responses over the global oceans. The CGCM results to Amazon deforestation, on the other hand, show enhanced local rainfall reduction and surface temperature increase relative to the AGCM results over the Amazon, in addition to significant remote responses. The CGCM also showed sensitivity to the spatial structure of the deforested/forested mesh size, with the smaller mesh deforestation scenario presenting larger rainfall reduction than the larger mesh scenario. We therefore speculate that not only the total amount, but also the continuity of forested areas are important for the convection process in the model. Such speculation must be further tested with higher resolution coupled ocean-atmosphere-biosphere global model.

The principal remote response detected with the CGCM experiments is an increased ENSO-like variability over the Pacific, due to ocean-atmosphere interactions originated by the Amazon forest clearing. The process is seen as a sequence of events as follows: The replacement of tropical rainforest for savanna in the coupled model interferes on local rainfall production, reducing the total annual rainfall over the deforested area; such reduction on Amazon deep convection would then act to reduce the trade winds, possibly through a reduction of the mean meridional atmospheric circulation and its impact on the subtropical high pressure systems (not shown); the relaxed trades over the central equatorial Pacific ocean impacts on oceanic circulation through the relaxation of both surface current system and the subtropical-tropical circulation cells, reducing equatorial upwelling, and therefore increasing the mean surface temperature over the eastern Pacific; the relaxation of the westward surface currents also impact on the depth and strength of the equatorial undercurrent, which results in enhanced advection of warm waters eastward. The warmer eastern Pacific then becomes a preferred state to displace the maritime convection from the western Pacific to the central and eastern portions of the basin, thus creating a state prone to the increased rainfall close to the South American continent due to the incursion of warm ENSO episodes; such displacement of the warm-pool atmospheric convection eastward over the Pacific increases the equatorially trapped zonal atmospheric circulation cell, inducing enhanced large scale subsidence over the Amazon rainforest, and thus further reducing rainfall there.

The upper ocean circulation response to idealized winds are a well known dynamical process and has been widely discussed in the literature (e.g., see Philander 1990, Figure 4.10). Yet, the results presented here differ from the case of prescribed idealized wind field on the OGCM. The wind field in the deforestation experiment is spatially and temporally modified according to non-linear interactions between the OGCM and AGCM in the coupled model as a result of a controlled change of continental

vegetation cover over the Amazon.

Another aspect emerging from this coupled modeling research is the lack of a linear relationship between rainfall departures over the eastern Pacific and the extent of deforested area over the Amazon, as depicted in Figure 4. Over the Amazon, the surface temperature departures are nearly time invariant and directly proportional to the extent of deforested area. Thus the linear relation with rainfall departures over the continent, the rational for that being the local reduction of evapo-transpiration and increased atmospheric static stability (e.g. Nobre et al., 1991). While over the Pacific, surface temperature departures are time dependent and a function of both atmospheric forcing and equatorial ocean dynamics (Schopf and Suarez, 1991). So, we see the chain of events started with the modulation of Amazon convection variations as a triggering mechanism to the more complex ocean-atmosphere interactions and ocean wave dynamics over the equatorial Pacific, which contribute for the rainfall modulation there.

Although the sequence of events described here is suggestive of a positive feedback between Amazon deforestation and equatorial Pacific ocean-atmosphere interactions resembling the ENSO phenomena, care must be exercised with such inference, since a number of approximations used (e.g., the arbitrary patterns of deforestation and the limited latitudinal extent of ocean-atmosphere coupling) and systematic errors of the GCMs used could either damp or exacerbate the model responses presented.

We believe that two main reasons may have contributed for other coupled ocean-atmosphere studies not identifying the further Amazon rainfall reduction due to ocean coupling. One is the dry bias over the Amazon shown by some studies (e.g. Schneider et al, 2006; Voldoire and Royer, 2005) and the use of anomaly-coupling strategies (e.g. in Schneider et al, 2006), which impede the coupled model to change its forced run mean state; e.g., not allowing the shallowing of the Pacific EUC due to the relaxation of the surface winds mean state. It is therefore our opinion that a fully coupled model (in the sense of no flux-correction) is a necessity to allow for more vigorous feedback processes to develop.

Last, but not least, despite the importance of biosphere-atmosphere-ocean interactions for global climate variability and change highlighted by the modeling framework used in this work, it must be kept in mind that the rainfall product of GCMs are but the result of parameterized algorithms, which ignore the very nature of rainfall and its complex biogeochemical dependencies. The global climate responses to tropical forest removal should be reevaluated with higher resolution, better physical parameterized, fully coupled global GCMs and, further down, when cloud-resolving Earth System models are accessible and the physics of rain drop growth is better known.

Acknowledgments

The authors acknowledge Dr. Francis Wagner for the vegetation maps provided and the anonymous reviewers for their constructive criticisms, that helped sharpen this paper's findings. The first author also acknowledges Mr. Ismael Nobre for the discussions during the first author's visit to Parque Nacional do Iguaçu, where this article was first drafted. The authors acknowledge use of GrADS (http://www.iges.org/grads/) and Ferret (http://ferret.pmel.noaa.gov/Ferret/) programs for the analysis and graphics in this paper. This research was partially funded by Fundação de Amparo à Pesquisa do Estado de São Paulo – FAPESP, under grants No. 2005/00915-2 and 2006/06241-6.

References

Cavalcanti, I. F. A., J. A. Marengo, P. Satyamurty, C. A. Nobre, I. Trosnikov, J. P. Bonatti, A. O. Manzi, T. Tarasova, C. D'Almeida, B. Sampaio, L. P. Pezzi, C. C. Castro, M. Sanches, and H. Camargo, 2002: Global climatological features in a simulation using CPTEC/COLA AGCM. *J. Climate,* **15,** 2965-2988.

De Vries, P., and K. Döös, 2001: Calculating Lagrangian trajectories using time-dependent velocity fields. *J. Atmos. Oceanic Technology,* **18,** 1092-1101.

Findell, K. L., T. R. Knudson, and P. C. D. Milly, 2006: Weak simulated extratropical responses to complete tropical deforestation. *J. Climate*, **19**, 2835-2850.

Giarolla, E., P. Nobre, M. Malagutti, and L. P. Pezzi, 2005: The Atlantic Equatorial Undercurrent: PIRATA observations and simulations with GFDL Modular Ocean Model at CPTEC. *Geophys. Res. Lett.,* **32,** L10617.

Harshvardhan, R. Davies, D. A. Randall, and T. G. Corsetti, 1987: A fast radiation parameterization for atmospheric circulation models. *J. Geophys. Res.,* **92,** 1009-1016.

Henderson-Sellers, A., and V. Gornitz, 1984: Possible climatic impacts of land cover tranformations, with particular emphasis on tropical deforestation. *Clim. Change,* **6,** 231-258.

Katz, E. J., 1987: Seasonal response of the sea surface to the wind in the equatorial Atlantic. *J. Geophys. Res.,* **92,** 1885-1893.

Lacis, A. A., and J. D. Hansen, 1974: A parameterization of the absortion of solar radiation in the Earth's atmosphere. *J. Atmos. Sci.,* **31,** 118-133.

Levitus, S., 1982: Climatological Atlas of the World Ocean. NOAA/ERL GFDL, Professional Paper 13, (NTIS PB83-184093), 1982.

Lorenz, E. N., 1956: Empirical Orthogonal Functions and statistical weather prediction. Dept. of Meteorology, Massachusetts Institute of Technology, **1**, Statistical Forecasting Project, 52 pp.

Mellor, G. L., and T. Yamada, 1982: Development of a turbulence closure model for geophysical fluid problems. *Reviews of Geophyis. and Space Physics,* **20,** 851-875.

Moorthi, S., and M. J. Suarez, 1992: Relaxed Arakawa-Schubert: A parameterization of moist convection for general circulation models. *Mon. Wea. Rev.,* **120,** 978-1002.

Nobre, C. A., P. J. Sellers, and J. Shukla, 1991: Amazonian deforestation and regional climate change. *J. Climate,* **4,** 957-988.

Nobre, P., and J. Shukla, 1996: Variations of sea surface temperature, wind stress, and rainfall over the tropical Atlantic and South America. *J. Climate,* **9,** 2464-2479.

Oberhuber, J. M., 1988: An atlas based on the "COADS" data set: The budget of heat, buoyancy and turbulent kinetic energy at the surface of the global ocean. Max-Planck Institute for Meteorology (MPI), Report No. 15, MPI, Hamburg, Germany.

Pacanowski, R. C., and S. M. Griffies, 1999: The MOM3 Manual. GFDL Ocean Group Technical Report No. 4, Princeton, NJ: *NOAA*/*Geophysical Fluid Dynamics Laboratory*, 680 pp.

Pacanowski, R. C., and S. G. H. Philander, 1981: Parameterization of vertical mixing in numerical models of tropical oceans. *J. Phys. Oceanography,* **11,** 1443-1451.

Philander, S. G. H., 1990: *El Niño, La Niña, and the Southern Oscillation,* Academic Press, 293 pp.

Preisendorfer, R. W., 1988: *Principal component analysis in meteorology and oceanography,* Elsevier, 452 pp.

Ramaswamy, V., and S. M. Freidenreich, 1992: A study of broadband parameterizations of the solar radiative interactions with water vapor and water drops. *J. Geophys. Res.,* **97,** 11487-11512.

Ramos da Silva, R., D. Werth, and R. Avissar, 2008: Regional impacts of future land-cover changes on the Amazon basin wet-season climate. *J. Climate,* **21,** 1153-1170.

Reynolds, R. W., N. A. Rayner, T. M. Smith, D. C. Stokes, and W. Wang, 2002: An improved in situ and satellite SST analysis for climate. *J. Climate,* **15,** 1609-1625.

Richter I. And S. Xie, 2008: On the origin of equatorial Atlantic biases in coupled general circulation models. *Climate Dynamics,* **31**, 587.

Rosati, A., and K. Miyakoda, 1988: A general circulation model for upper ocean simulation. *J. Phys. Ocean.,* **18,** 1601-1626.

Schneider, E. K., M. Fan, B. P. Kirtman, and P. A. Dirmeyer, 2006: Potential effects of Amazon deforestation on tropical climate. IGES/COLA, 41 pp.

Schopf, P. S. and M. J. Suarez, 1991: Ocean wave dynamics and the time scale of ENSO. *J. Phys. Oceanogr.* **20**, 629-645.

Snowden, D., and R. L. Molinari, 2003: Subtropical cells in the Atlantic Ocean: An observations summary. In: *Interhemispheric Water Exchange in the Atlantic Ocean*, G. G. a. P. Malanotte-Rizzoli Ed., p.p. 287-312, Elsevier Oceanography Series, Amsterdam.

Stephenson, D. B. and R. E. Benestad, 2009: Environmental statistics for climate researchers. http://folk.uib.no/ngbnk/kurs/notes/node52.html

Trenberth, K. E., J. G. Olson, and W. G. Large, 1989: A global ocean wind stress climatology based on ECMWF analyses. NCAR, NCAR/TN-338+STR, 93 pp.

Voldoire, A., and J.-F. Royer, 2005: Climate sensitivity to tropical land surface changes with coupled versus prescribed SSTs. *Climate Dynamics,* **24,** 843-862.

Werth, D., and R. Avissar, 2002: The local and global effects of Amazon deforestation. *J. Geophys. Res.,* **107,** 8087, doi:10.1029/2001JD00717.

Xie, S. P., 1994: Oceanic Response to the Wind Forcing Associated with the Intertropical Convergence Zone in the Northern-Hemisphere. *Journal of Geophysical Research-Oceans,* **99,** 20393-20402.

Xue, Y., P. J. Sellers, J. L. K. III, and J. Shukla, 1991: A simplified biosphere model for global climate studies. *J. Climate,* **4,** 345-364.

Zeng, N., R. E. Dickinson, and X. Zeng, 1996: Climatic impact of Amazon deforestation - A mechanistic model study. *J. Climate,* **9,** 859-883.

Figure Captions:

Figure 1 - Vegetation cover types over South America as used for the (a) Control, and deforestation experiments (b) 50% on 1.85° x 1.85° meshes, (c) 50% on 5.5° x 5.5° meshes, and (d) 100% on one single mesh. The colors indicate the type of vegetation used; light green indicates savanna-type vegetation and dark purple indicates broad-leaf evergreen trees (see: Xue et al., 1991 Table 2 for a complete listing of vegetation types).

Figure 2 – (a) First joint EOF spatial pattern for the SST and surface wind stress anomalies for the 200-year time series of the CTRL experiment, explaining 14.7% of the combined fields total variance: SST (shaded), and surface wind stress (arrows) presented as correlation maps. (b) Power spectra of the principal components time series for the eigenvector shown in (a) (continuous line) and for the DFOR3 case, explaining 15.1% of the total variance (figure not shown) (dashed line).

Figure 3 – Annual cycle of area averaged precipitation long term mean over the central Amazon area for (a) AGCM and (b) CGCM for each model's CTRL (continuous black line), DFOR1 (dashed lines), DFOR2 (dotted lines) and DFOR3 (dotted-dashed line) experiments. The continuous red line represents observed climatological rainfall over the same area, from NOAA CAMS/OPI precipitation product. Units are mm/day.

Figure 4 - Ensemble mean precipitation departures area averaged over central Amazon (a, c) and Niño 3.4 area (b, d), for the AGCM (a, b) and CGCM (c, d) experiments. DFOR1 (blue lines), DFOR2 (red lines), and DFOR3 (black lines). Units are mm/day. Time series are smoothed with 11 months running mean averages. The horizontal dotted color lines represent the 20-year average of each experiment departures.

Figure 5 – 20-year mean ensemble DFOR3 departures: precipitation (left column), in mm/day, and near surface air temperature (right column), in degree C, for the AGCM (top row), CGCM (center row), and the residual CGCM minus AGCM departures (bottom row). Statistically significant departures at the 95% level are shaded.

Figure 6 – Annual mean zonally averaged zonal velocities between 180W and 100W: (a) vertically averaged on the top 20 m from the CTRL experiment (continuous black line – cm/s, see text for current acronyms), DFOR3 departures (continuous blue line – cm/s), and DFOR3 surface wind stress amplitude departures (red dashed line – N/m2); and (b) vertical profiles of the zonally averaged zonal velocities from CTRL (black contours) and DFOR3 departures statistically significant at the 95% level (shaded).

Figure 7 – Vertical velocity component (cm/day) for the CTRL experiment at 50 m depth (black contours - positive values represent upwelling) and DFOR3 departures statistically significant at the 95% level (shades).

Figure 8 - Temperature (degree C) depth-longitude cross section along the equator for the CTRL experiment (black continuous contours), DFOR3 experiment (black dashed contours), and DFOR3 departures statistically significant at the 95% level (shades).

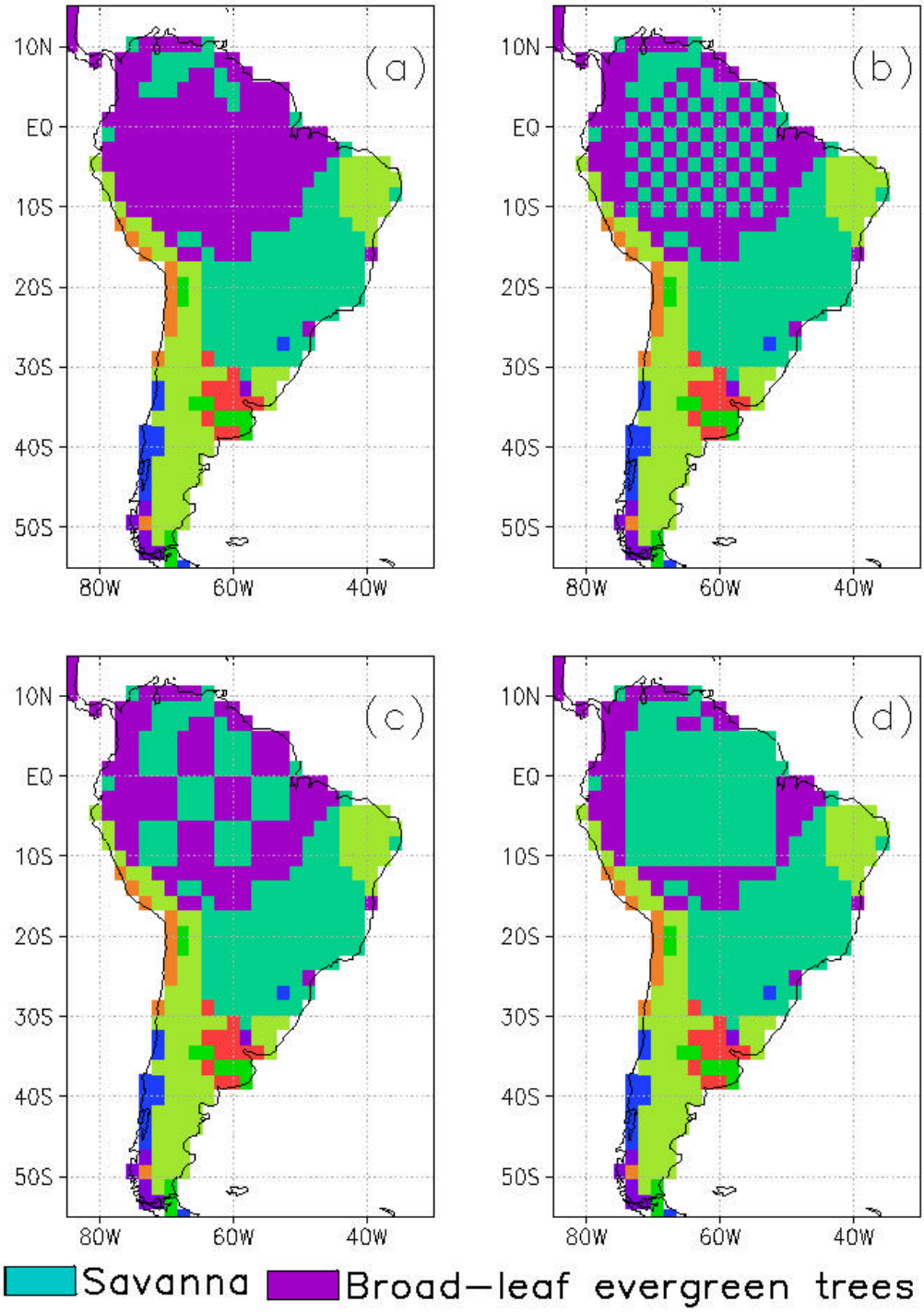

Figure 1 - Vegetation cover types over South America as used for the (a) Control, and deforestation experiments (b) 50% on 1.85° x 1.85° meshes, (c) 50% on 5.5° x 5.5° meshes, and (d) 100% on one single mesh. The colors indicate the type of vegetation used; light green indicates savanna-type vegetation and dark purple indicates broad-leaf evergreen trees (see: Xue et al., 1991 Table 2 for a complete listing of vegetation types).

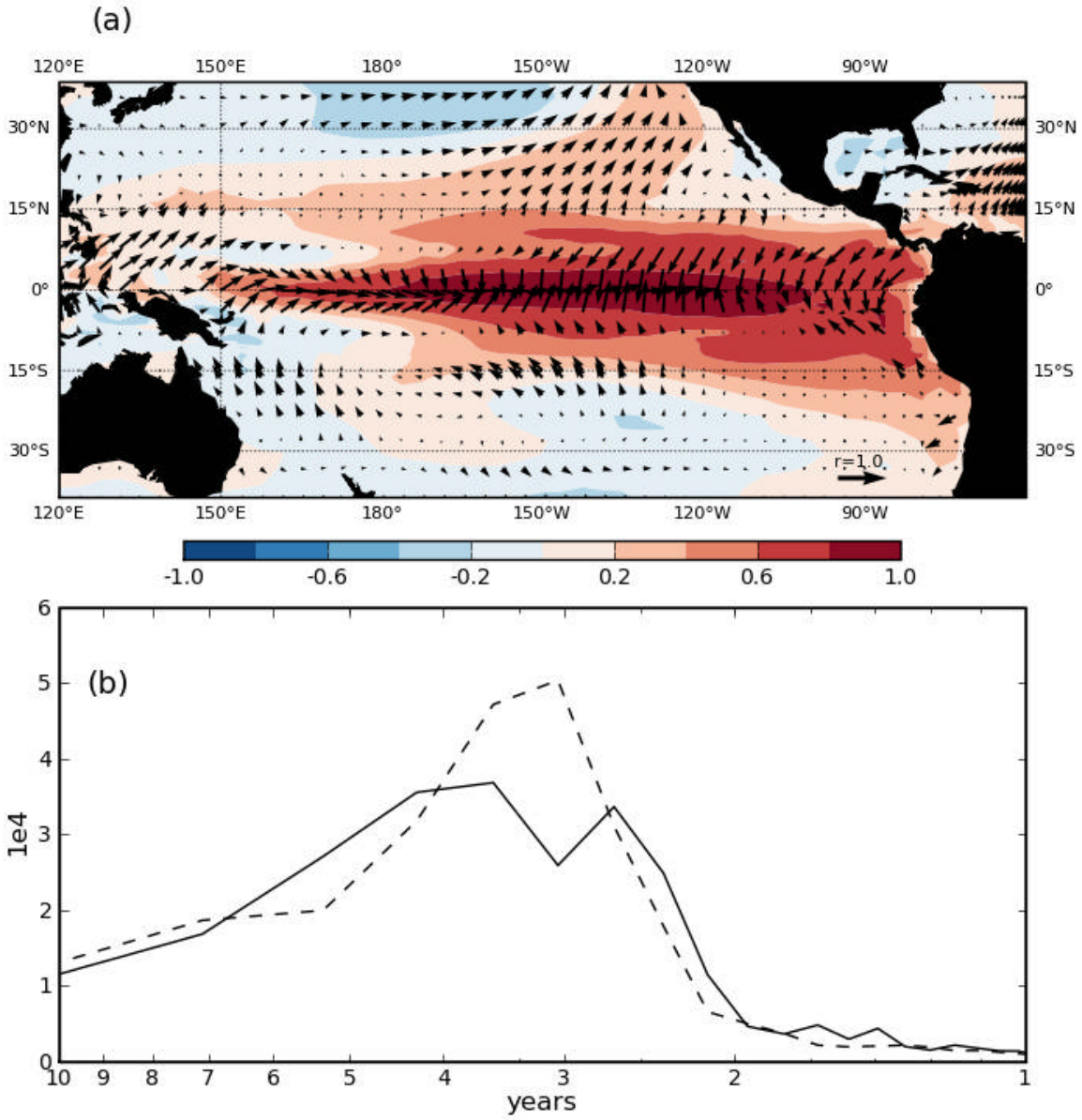

Figure 2 – (a) First joint EOF spatial pattern for the SST and surface wind stress anomalies for the 200-year time series of the CTRL experiment, explaining 14.7% of the combined fields total variance: SST (shaded), and surface wind stress (arrows) presented as correlation maps. (b) Power spectra of the principal components time series for the eigenvector shown in (a) (continuous line) and for the DFOR3 case, explaining 15.1% of the total variance (figure not shown) (dashed line).

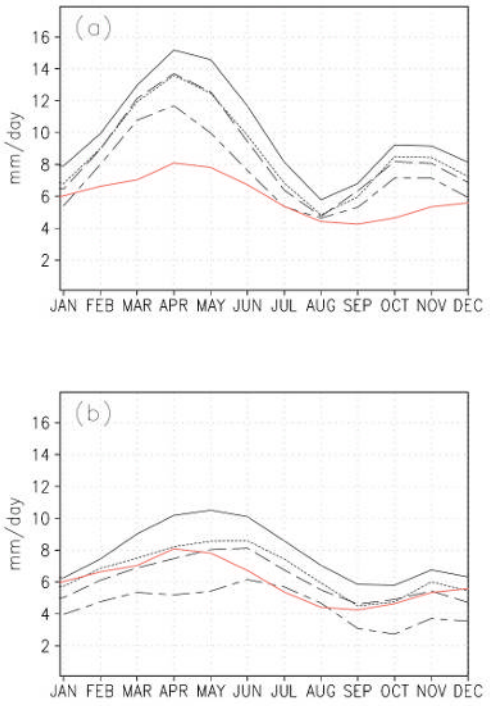

Figure 3 – Annual cycle of area averaged precipitation long term mean over the central Amazon area for (a) AGCM and (b) CGCM for each model's CTRL (continuous black line), DFOR1 (dashed lines), DFOR2 (dotted lines) and DFOR3 (dotted-dashed line) experiments. The continuous red line represents observed climatological rainfall over the same area, from NOAA CAMS/OPI precipitation product. Units are mm/day.

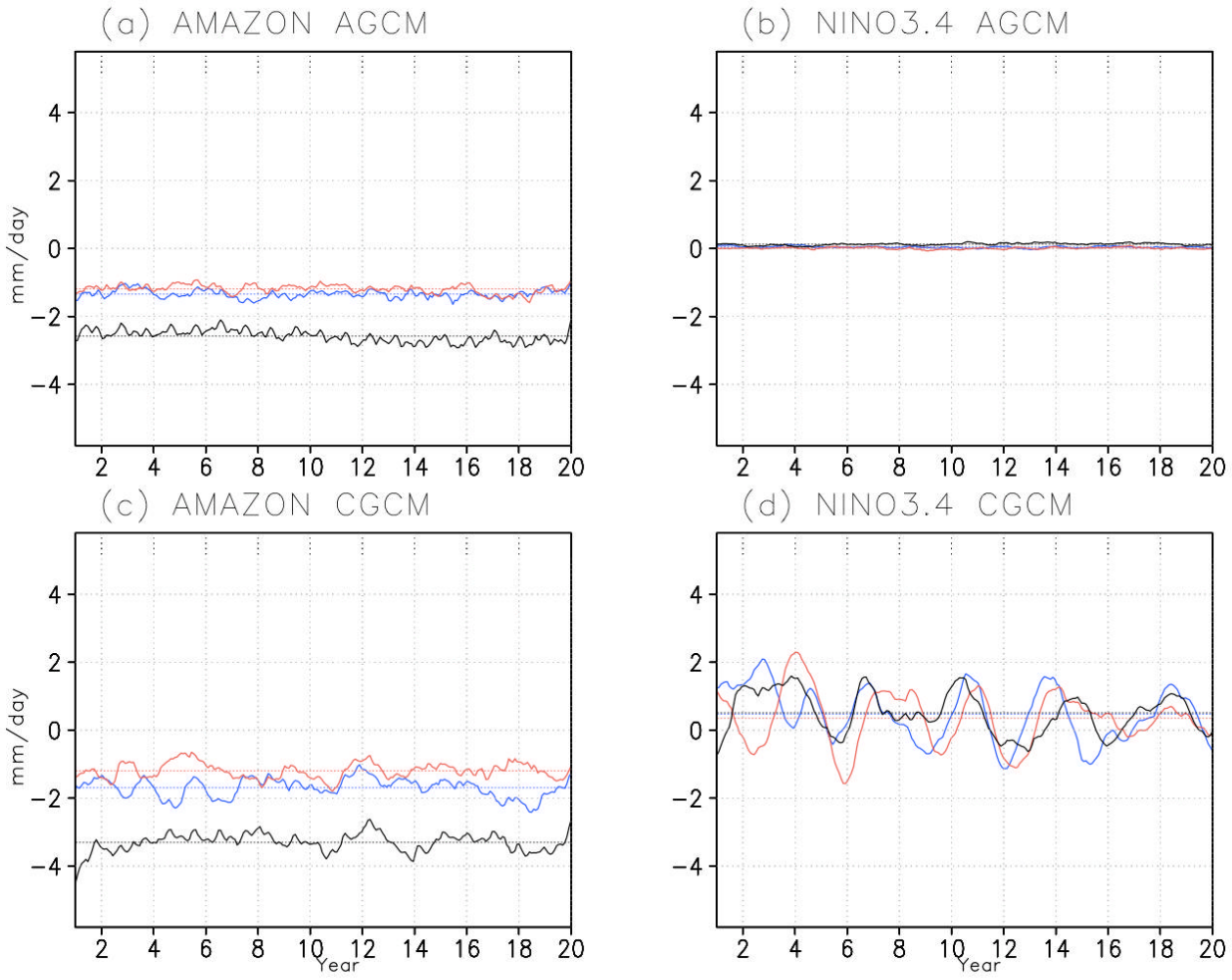

Figure 4 - Ensemble mean precipitation departures area averaged over central Amazon (a, c) and Niño 3.4 area (b, d), for the AGCM (a, b) and CGCM (c, d) experiments. DFOR1 (blue lines), DFOR2 (red lines), and DFOR3 (black lines). Units are mm/day. Time series are smoothed with 11 months running mean averages. The horizontal dotted color lines represent the 20-year average of each experiment departures.

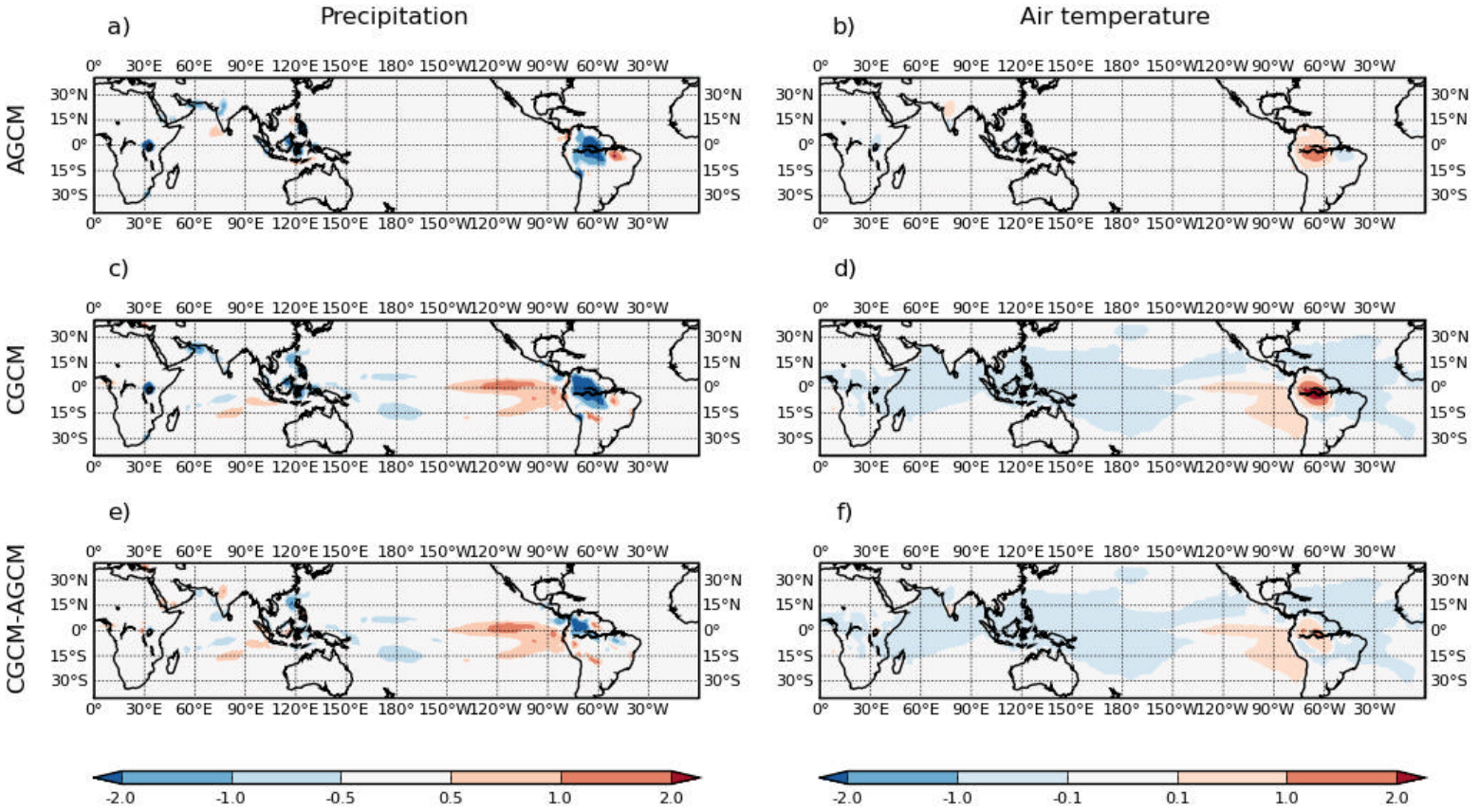

Figure 5 – 20-year mean ensemble DFOR3 departures: precipitation (left column), in mm/day, and near surface air temperature (right column), in degree C, for the AGCM (a, b), CGCM (c, d), and the residual CGCM minus AGCM departures (e, f). Statistically significant departures at the 95% level are shaded.

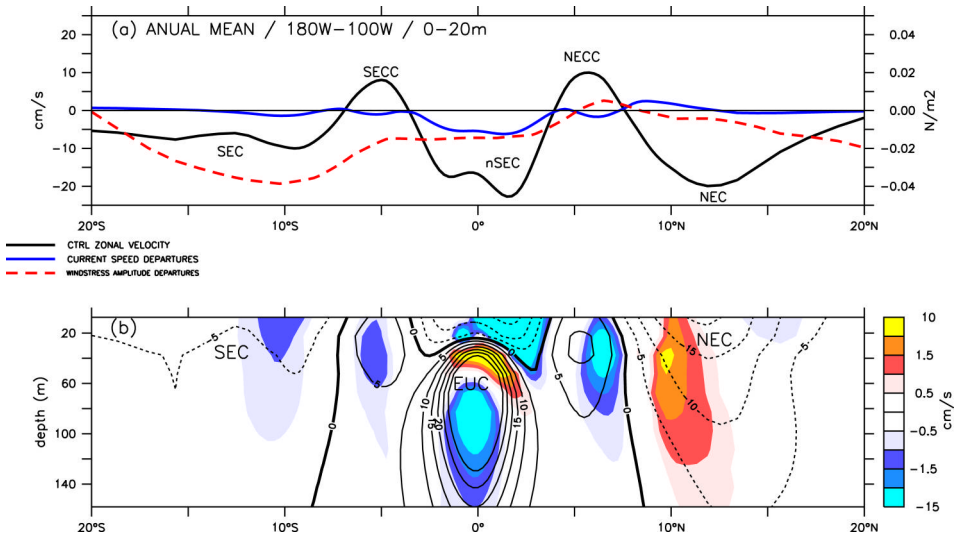

Figure 6 - Annual mean zonally averaged zonal velocities between 180W and 100W: (a) vertically averaged on the top 20 m from the CTRL experiment (continuous black line – cm/s, see text for current acronyms), DFOR3 departures (continuous blue line – cm/s), and DFOR3 surface wind stress amplitude departures (red dashed line – N/m2); and (b) vertical profiles of the zonally averaged zonal velocities from CTRL (black contours) and DFOR3 departures statistically significant at the 95% level (shaded).

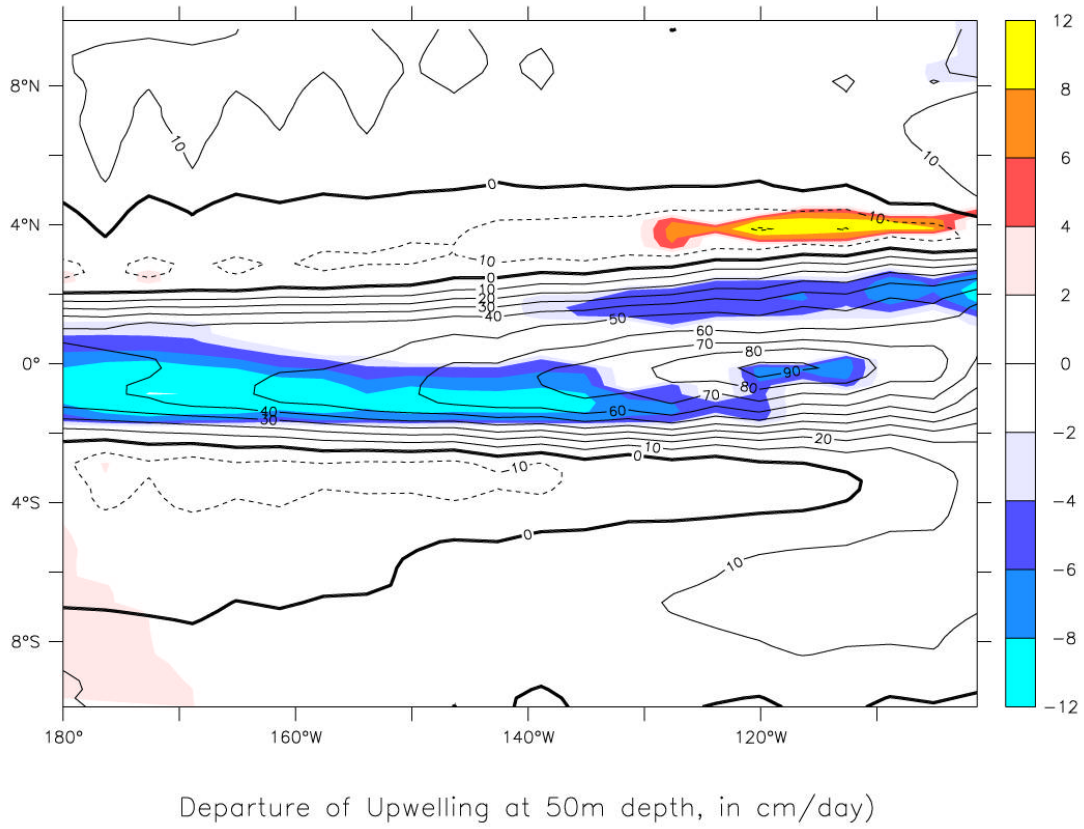

Figure 7 - Vertical velocity component (cm/day) for the CTRL experiment at 50 m depth (black contours - positive values represent upwelling) and DFOR3 departures statistically significant at the 95% level (shades).

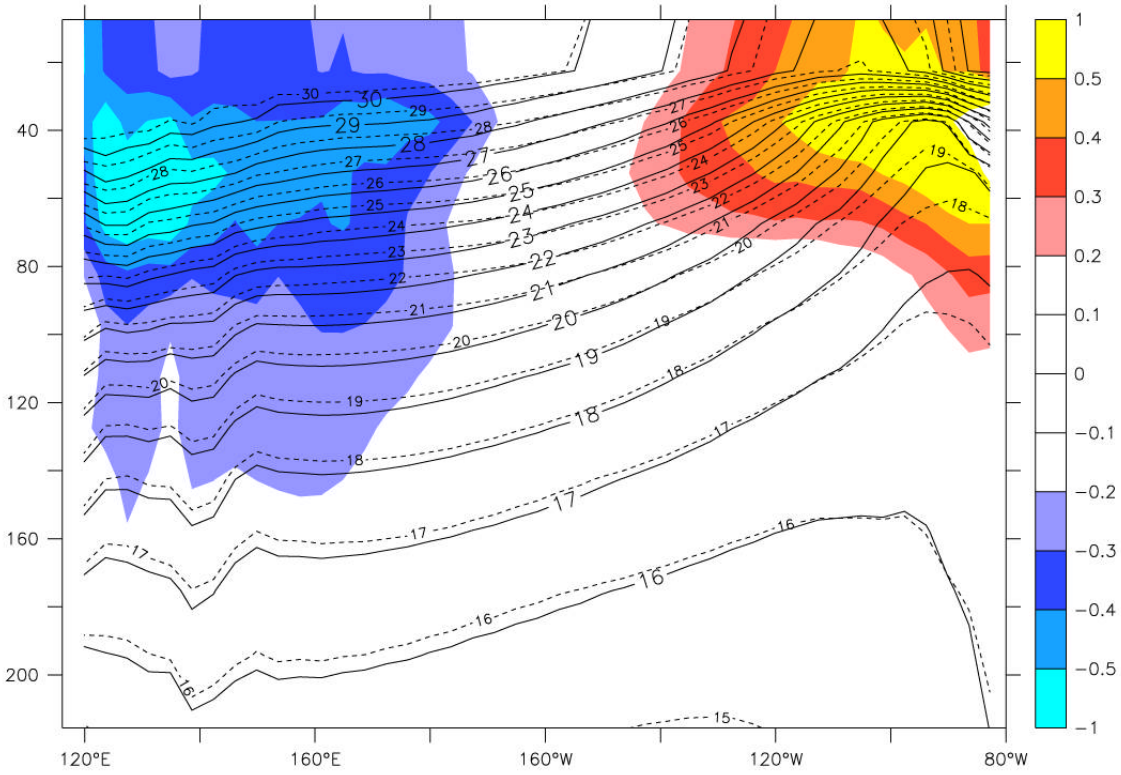

Figure 8 - Temperature (degree C) depth-longitude cross section along the equator for the CTRL experiment (black continuous contours), DFOR3 experiment (black dashed contours), and DFOR3 departures statistically significant at the 95% level (shades).

Experi-ment	AMAZON				NIÑO 3.4			
	MEAN (mm)		STDEV (mm)		MEAN (mm)		STDEV (mm)	
	AGCM	CGCM	AGCM	CGCM	AGCM	CGCM	AGCM	CGCM
DFOR1	-1.341 (-13.5%)	-1.693 (-21.6%)	0.121	0.283	0.041 (2.1%)	0.478 (9.1%)	0.029	0.792
DFOR2	-1.190 (-12.0%)	-1.963 (-15.3%)	0.127	0.230	0.007 (0.3%)	0.350 (6.6%)	0.028	0.806
DFOR3	-2.580 (-26.1%)	-3.303 (-42.2%)	0.179	0.269	0.125 (6.3%)	0.513 (9.7%)	0.033	0.609

Table 1 – Area averaged precipitation departures (deforestation minus CTRL) over the central Amazon and the Niño 3.4 areas for the AGCM and CGCM long term mean (shown as straight color lines in Figure 4); values in parenthesis are in percent of the experiment's total annual rainfall amount for the respective experiment and model. The columns “STDEV” show the standard deviations of the departures time series about their respective long term mean values.